Hindawi Publishing Corporation
Advances in Physical Chemistry
Volume 2012, Article ID 572148, 20 pages
doi:10.1155/2012/572148

Research Article

Ab Initio Potential Energy Surfaces for Both the Ground ($\widetilde{X}^1A'$) and Excited ($\widetilde{A}^1A''$) Electronic States of HSiBr and the Absorption and Emission Spectra of HSiBr/DSiBr

Anyang Li,[1,2] Sen Lin,[1] and Daiqian Xie[1]

[1] *Institute of Theoretical and Computational Chemistry, Key Laboratory of Mesoscopic Chemistry, School of Chemistry and Chemical Engineering, Nanjing University, Nanjing 210093, China*
[2] *Institute of High Performance Computing and Applications, Chongqing University of Posts and Telecommunications, Chongqing 400065, China*

Correspondence should be addressed to Daiqian Xie, dqxie@nju.edu.cn

Received 27 May 2011; Accepted 14 July 2011

Academic Editor: Xinchuan Huang

Ab initio potential energy surfaces for the ground ($\widetilde{X}^1A'$) and excited ($\widetilde{A}^1A''$) electronic states of HSiBr were obtained by using the single and double excitation coupled-cluster theory with a noniterative perturbation treatment of triple excitations and the multireference configuration interaction with Davidson correction, respectively, employing an augmented correlation-consistent polarized valence quadruple zeta basis set. The calculated vibrational energy levels of HSiBr and DSiBr of the ground and excited electronic states are in excellent agreement with the available experimental band origins. In addition, the absorption and emission spectra of HSiBr and DSiBr were calculated using an efficient single Lanczos propagation method and are in good agreement with the available experimental observations.

1. Introduction

Silylenes and its halogenated analogs are important reactive intermediates in the chemical vapor deposition of silicon thin films [1] and plasma etching process [2]. The identification and quantification of such intermediates could help make these processes more efficient, so that they have attracted much attention in experimental and theoretical studies [3–17]. However, because these radicals are typically short-lived and highly reactive, it is difficult to monitor them. Due to the lack of comprehensive spectroscopic signatures for these species, the detailed mechanism of such semiconductor growth processes is still not fully understood.

In this work, we focus on the monobromosilylene (HSiBr) system, which was first detected by Herzberg and Verma in 1964 [3]. Both absorption and emission spectra of HSiBr in the 410–600 nm were obtained by flash photolysis of SiH_3Br. The vibrational fundamentals and geometries for both the ground and excited states were confirmed after vibrational and rotational analyses of the spectra. Although no spin splittings were observed, the occurrence of subbands with $\Delta K = 0$ and ± 2 led them to assume that the electronic transition was triplet-singlet. Subsequently in 1965, these electronic transitions were confirmed to be $\widetilde{A}^1A'' - \widetilde{X}^1A'$ by Hougen and Watson via an "axis-switching" mechanism [4]. The spectra of the $\widetilde{A}^1A'' - \widetilde{X}^1A'$ system of jet-cooled HSiBr and its deuterated analog were obtained about 15 years ago by Harjanto et al. [8] using pulsed electric discharge techniques, and the r_0 structures for the ground and excited states were determined from the rotational analyses of the 0_0^0 band. Later in 2001, 26/51 ground state vibrational levels of HSiBr/DSiBr were observed by Hostutler et al. [13] from the single vibronic level dispersed fluorescence spectra of jet-cooled HSiBr/DSiBr by laser excitation of selected bands.

Unlike HSiF and HSiCl, only a few theoretical studies have been reported for monobromosilylene (HSiBr) [6, 13]. In 1979, Gilchrist et al. [6] determined the geometrical structures and bending potentials for the excited state $\widetilde{A}^1A''$ of HSiBr by fitting the Herzberg and Verma's data [3] and also obtained the H–Si stretching frequency($\nu_1' = 1785\,\mathrm{cm}^{-1}$),

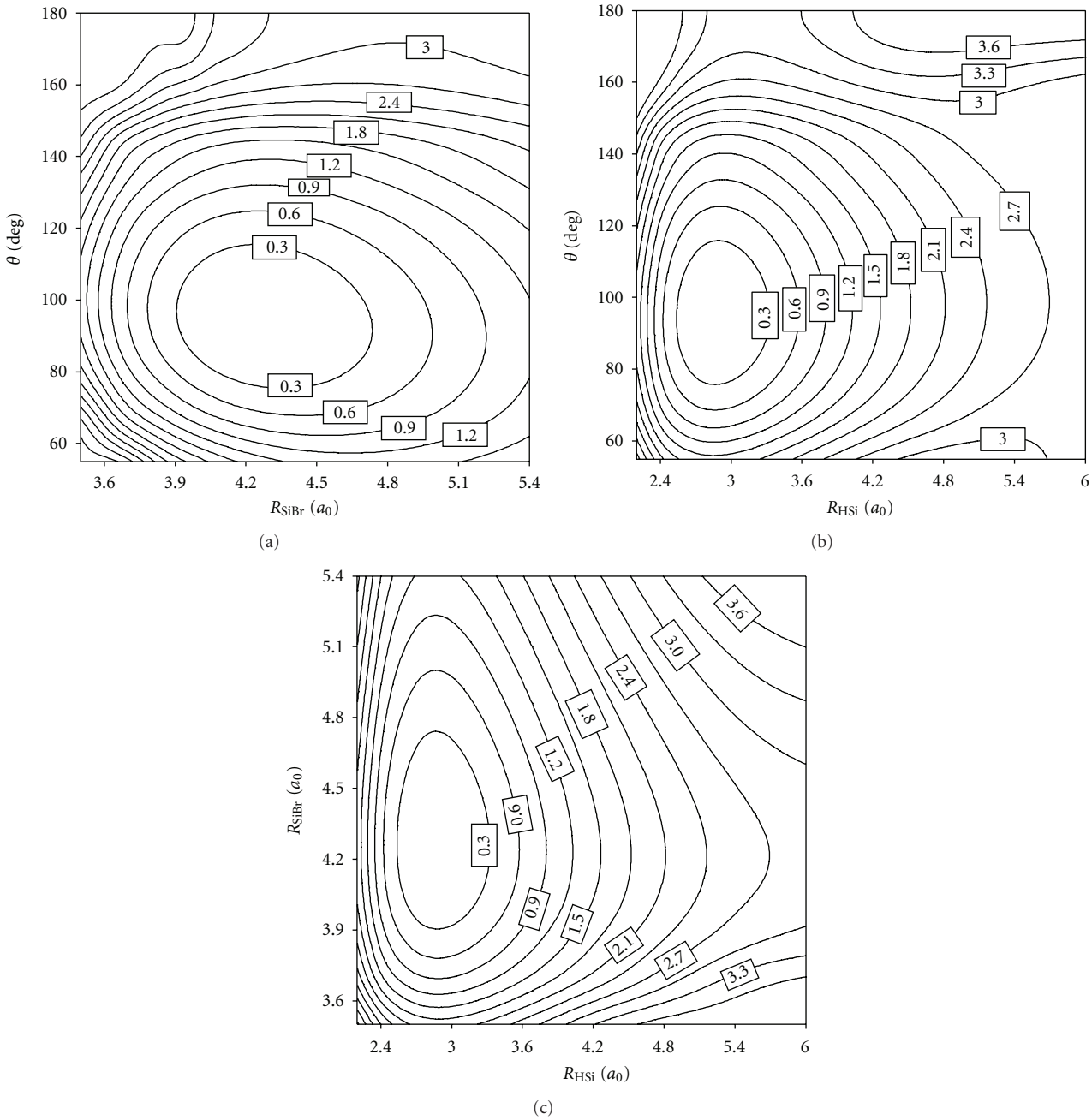

Figure 1: Contour plots of the potential energy surface of HSiBr($\tilde{X}^1A'$) in the internal coordinates. (a) Contour plot at $R_{HSi} = 2.869\,a_0$. (b) Contour plot at $R_{SiBr} = 4.257\,a_0$. (c) Contour plot at $\theta = 93.9°$. Contours are spaced by 0.3 eV with the zero defined at the HSiBr($\tilde{X}^1A'$) minimum.

which is agreement with the later experimental value of $1787\,\text{cm}^{-1}$ [8]. In order to ascertain the validity of their refined force constants, Hostutler et al. [13] calculated the independent ground and excited state structures at B3LYP level with 6-311G(3df,3pd) basis set in 2001. To our best knowledge, however, no potential energy surface (PES) has been reported for either the ground or excited electronic state of HSiBr. The lack of reliable PESs will hinder our understanding of the spectroscopy of this important molecule, particularly for highly excited vibrational levels which can be probed by emission spectroscopy.

In the present work, we extend our previous studies on the HGeCl [18], HGeBr [19], and HSiCl [20] systems by reporting accurate *ab initio* PESs for both the ground ($\tilde{X}^1A'$) and excited ($\tilde{A}^1A''$) electronic states of HSiBr using the coupled cluster singles and doubles with perturbative triples method [CCSD(T)] and the internally contracted multireference configuration interaction method with the

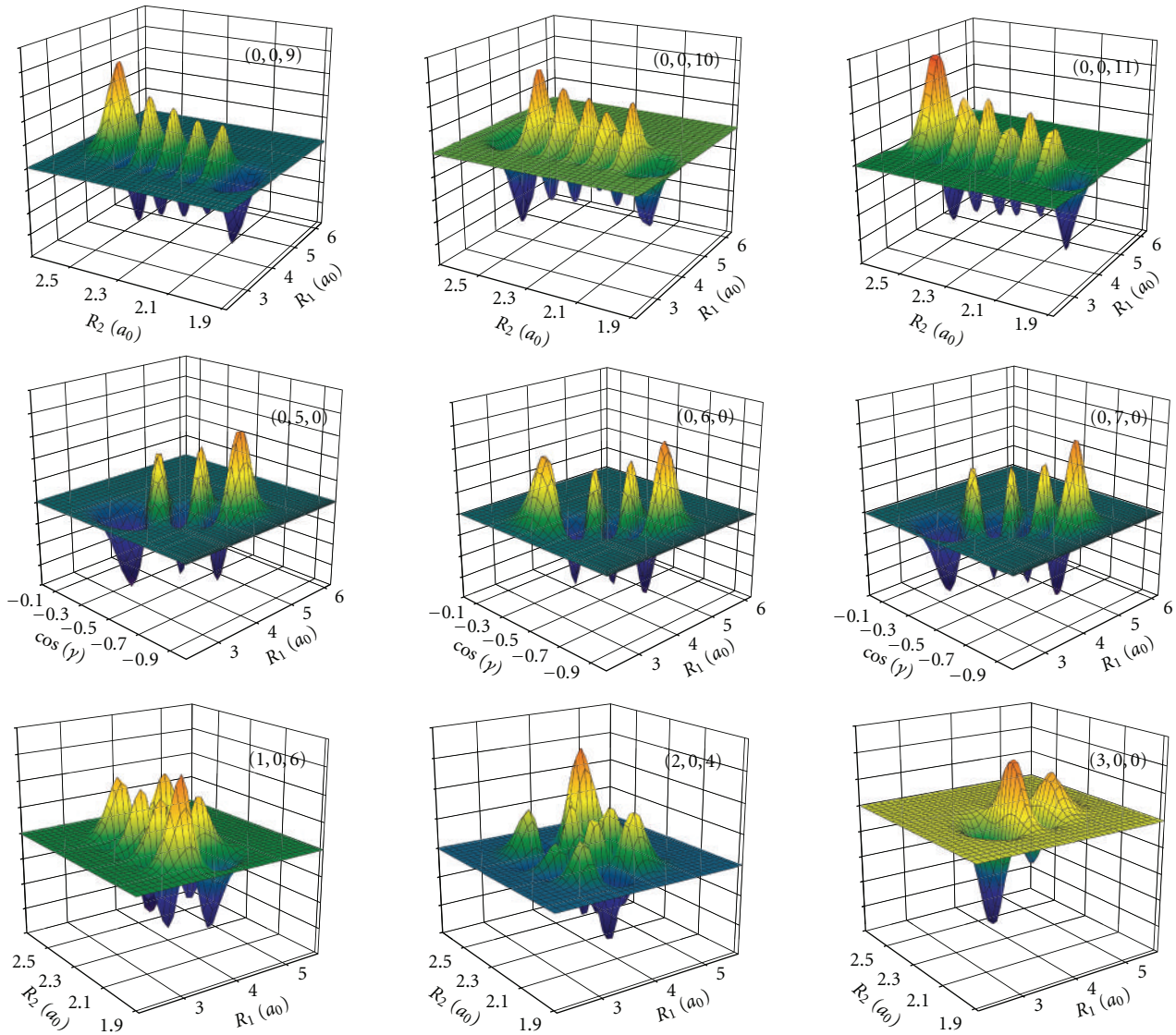

Figure 2: Nine vibrational wave functions of HSiBr ($\tilde{X}^1A'$) in the Radau coordinates. The three vibrational quantum numbers (n_1, n_2, n_3) represent the H–Si stretching, bending, and Si–Br stretching modes, respectively.

Table 1: Geometrical parameters for the ground and excited states of HSiBr.

Electronic state	Method	R_e(HSi) (Å)	R_e(SiCl) (Å)	θ_e(HSiCl) (°)
$\tilde{X}^1A'$	CCSD(T)/AVQZ[a]	1.518	2.253	93.9
	B3LYP/6-311G(3df,3pd)[b]	1.524	2.2674	94.3
	Expt.[c]	1.561	2.231	102.9
	Expt.[d]	1.518	2.237	93.4
	Expt.[b]	1.503	2.235	92.8
$\tilde{A}^1A''$	CAS/MRCI +Q/AVQZ[a]	1.499	2.219	117.7
	B3LYP/6-311G(3df,3pd)[b]	1.5014	2.2339	115.9
	Expt.[c]	1.499	2.208	116.6
	Expt.[d]	1.497	2.208	116.4

[a]This work.
[b]Reference [13].
[c]Reference [3].
[d]Reference [8].

Table 2: Calculated vibrational energy levels (in cm^{-1}) and comparison with available experimental results for HSiBr ($\widetilde{X}^1A'$).

(n_1, n_2, n_3)	This work	Expt. [13]	(n_1, n_2, n_3)	This work	Expt. [13]
(0, 0, 0)	0.0		(2, 0, 4)	5509.4	
(0, 0, 1)	409.3	412.4	(1, 1, 7)	5528.3	
(0, 1, 0)	770.3	772.0	(1, 0, 9)	5569.3	
(0, 0, 2)	815.7		(0, 7, 1)	5668.2	5682.0
(0, 1, 1)	1176.7	1181.4	(0, 6, 3)	5706.5	
(0, 0, 3)	1219.5		(1, 5, 0)	5710.5	5717.8
(0, 2, 0)	1536.4	1540.7	(3, 0, 0)	5717.7	
(0, 1, 2)	1580.4		(0, 5, 5)	5742.8	
(0, 0, 4)	1620.7		(1, 4, 2)	5757.7	
(0, 2, 1)	1939.7	1946.3	(0, 4, 7)	5775.7	
(1, 0, 0)	1977.6	1976.2	(2, 2, 1)	5782.7	
(0, 1, 3)	1981.3		(0, 3, 9)	5803.7	
(0, 0, 5)	2019.3		(1, 3, 4)	5818.1	
(0, 3, 0)	2296.3	2301.1	(0, 2, 11)	5825.5	
(0, 2, 2)	2340.4		(0, 1, 13)	5841.9	
(0, 1, 4)	2379.5		(2, 1, 3)	5846.3	
(1, 0, 1)	2387.6	2386.7	(0, 0, 15)	5856.9	
(0, 0, 6)	2415.3		(1, 2, 6)	5871.6	
(0, 3, 1)	2696.4	2705.5	(2, 0, 5)	5908.4	
(1, 1, 0)	2734.8	2733.2	(1, 1, 8)	5917.0	
(0, 2, 3)	2738.3		(1, 0, 10)	5954.3	
(0, 1, 5)	2775.2		(0, 8, 0)	6017.4	6031.9
(1, 0, 2)	2794.6		(0, 7, 2)	6053.0	
(0, 0, 7)	2808.6		(0, 6, 4)	6088.9	
(0, 4, 0)	3050.2	3058.2	(1, 5, 1)	6090.2	
(0, 3, 2)	3094.0		(0, 5, 6)	6114.8	
(0, 2, 4)	3133.6		(2, 3, 0)	6124.3	
(1, 1, 1)	3142.2		(3, 0, 1)	6127.9	
(0, 1, 6)	3168.3		(0, 4, 8)	6153.1	
(1, 0, 3)	3198.9		(1, 4, 3)	6154.7	
(0, 0, 8)	3199.0		(0, 3, 10)	6179.7	
(0, 4, 1)	3447.0	3457.2	(2, 2, 2)	6183.3	
(1, 2, 0)	3487.7	3485.1	(0, 2, 12)	6198.7	
(0, 3, 3)	3489.0		(1, 3, 5)	6209.7	
(0, 2, 5)	3526.3		(0, 1, 14)	6213.5	
(1, 1, 2)	3546.5		(0, 0, 16)	6230.2	
(0, 1, 7)	3558.8		(2, 1, 4)	6244.6	
(0, 0, 9)	3586.6		(1, 2, 7)	6260.2	
(1, 0, 4)	3600.7		(1, 1, 9)	6300.1	
(0, 5, 0)	3798.7	3808.9	(2, 0, 6)	6307.4	
(0, 4, 2)	3841.5		(1, 0, 11)	6336.5	
(2, 0, 0)	3880.9	3881.4	(0, 8, 1)	6399.6	
(0, 3, 4)	3881.4		(0, 7, 3)	6435.9	
(1, 2, 1)	3893.8		(1, 6, 0)	6441.1	6449.8
(0, 2, 6)	3916.5		(3, 1, 0)	6444.6	
(0, 1, 8)	3946.4		(0, 6, 5)	6471.3	
(1, 1, 3)	3948.1		(2, 3, 1)	6485.0	
(0, 0, 10)	3971.4		(0, 5, 7)	6503.3	
(1, 0, 5)	3999.9		(1, 5, 2)	6516.2	
(0, 5, 1)	4192.1	4202.9	(0, 4, 9)	6530.9	

Table 2: Continued.

(n_1, n_2, n_3)	This work	Expt. [13]	(n_1, n_2, n_3)	This work	Expt. [13]
(0, 4, 3)	4233.3		(3, 0, 2)	6534.2	
(1, 3, 0)	4234.5	4234.5	(1, 4, 4)	6546.1	
(0, 3, 5)	4271.0		(0, 3, 11)	6552.8	
(2, 0, 1)	4288.1		(0, 2, 13)	6569.5	
(1, 2, 2)	4298.7		(2, 2, 3)	6581.6	
(0, 2, 7)	4304.0		(0, 1, 15)	6584.2	
(0, 1, 9)	4331.1		(1, 3, 6)	6598.5	
(1, 1, 4)	4347.0		(0, 0, 17)	6607.9	
(0, 0, 11)	4353.3		(2, 1, 5)	6639.7	
(1, 0, 6)	4396.5		(1, 2, 8)	6646.9	
(0, 6, 0)	4542.4	4557.8	(1, 1, 10)	6682.9	
(0, 5, 2)	4583.4		(2, 0, 7)	6701.0	
(2, 1, 0)	4622.1		(1, 0, 12)	6716.0	
(0, 4, 4)	4622.9		(0, 9, 0)	6748.4	
(1, 3, 1)	4639.7		(0, 8, 2)	6780.7	
(0, 3, 6)	4658.2		(2, 4, 0)	6813.7	
(0, 2, 8)	4688.8		(0, 7, 4)	6816.7	
(1, 2, 3)	4689.3		(1, 6, 1)	6844.5	
(2, 0, 2)	4703.9		(0, 6, 6)	6849.9	
(0, 1, 10)	4712.9		(3, 1, 1)	6850.7	
(0, 0, 12)	4732.6		(2, 3, 2)	6878.2	
(1, 1, 5)	4743.4		(0, 5, 8)	6879.5	
(1, 0, 7)	4790.4		(0, 4, 10)	6904.1	
(0, 6, 1)	4932.4	4946.5	(1, 5, 3)	6915.1	
(0, 5, 3)	4972.4		(0, 3, 12)	6923.2	
(1, 4, 0)	4975.2	4979.2	(1, 4, 5)	6931.1	
(0, 4, 5)	5009.6		(0, 2, 14)	6938.4	
(2, 1, 1)	5025.1		(3, 0, 3)	6942.6	
(0, 3, 7)	5042.9		(0, 1, 16)	6956.2	
(1, 3, 2)	5043.4		(2, 2, 4)	6977.2	
(0, 2, 9)	5070.6		(1, 3, 7)	6985.0	
(1, 2, 4)	5086.3		(0, 0, 18)	6995.9	
(0, 1, 11)	5091.9		(1, 2, 9)	7026.1	
(2, 0, 3)	5107.7		(2, 1, 6)	7036.7	
(0, 0, 13)	5109.4		(1, 1, 11)	7062.3	
(1, 1, 6)	5137.2		(2, 0, 8)	7092.1	
(1, 0, 8)	5181.3		(1, 0, 13)	7093.0	
(0, 7, 0)	5282.0	5229.1	(0, 9, 1)	7126.0	
(0, 6, 2)	5320.5		(0, 8, 3)	7160.2	
(0, 5, 4)	5358.4		(3, 2, 0)	7166.8	
(1, 4, 1)	5359.0		(1, 7, 0)	7167.4	7176.8
(2, 2, 0)	5380.0		(0, 7, 5)	7195.0	
(0, 4, 6)	5394.0		(2, 4, 1)	7207.6	
(2, 1, 2)	5423.5		(0, 6, 7)	7226.1	
(0, 3, 8)	5424.7		(1, 6, 2)	7244.4	
(1, 3, 3)	5445.8		(3, 1, 2)	7251.9	
(0, 2, 10)	5449.5		(0, 5, 9)	7252.9	
(0, 1, 12)	5468.1		(2, 3, 3)	7269.8	
(1, 2, 5)	5480.3		(0, 4, 11)	7274.5	
(0, 0, 14)	5483.9		(0, 3, 13)	7291.1	

Table 3: Calculated vibrational energy levels (in cm^{-1}) and comparison with available experimental results for DSiBr ($\widetilde{X}^1A'$).

(n_1, n_2, n_3)	This work	Expt. [13]	(n_1, n_2, n_3)	This work	Expt. [13]
(0, 0, 0)	0.0		(0, 4, 7)	4959.8	
(0, 0, 1)	405.0	407.99	(1, 5, 2)	4976.7	4981.7
(0, 1, 0)	562.0	561.8	(2, 1, 4)	4985.7	
(0, 0, 2)	807.2	812.4	(1, 0, 9)	4990.3	
(0, 1, 1)	965.0	968.5	(3, 0, 2)	5011.6	
(0, 2, 0)	1122.1	1121.3	(0, 2, 10)	5015.8	
(0, 0, 3)	1206.8		(2, 4, 0)	5021.4	
(0, 1, 2)	1365.4	1371.5	(0, 7, 3)	5042.3	
(1, 0, 0)	1439.7	1439.5	(0, 0, 13)	5059.6	
(0, 2, 1)	1523.2	1528.7	(1, 3, 5)	5067.1	
(0, 0, 4)	1603.9		(0, 5, 6)	5117.4	
(0, 3, 0)	1678.9	1679.6	(1, 6, 1)	5122.4	
(0, 1, 3)	1763.1		(2, 2, 3)	5131.8	
(1, 0, 1)	1844.7	1844.9	(1, 1, 8)	5145.2	
(0, 2, 2)	1921.7	1927.9	(3, 1, 1)	5150.8	
(1, 1, 0)	1995.5	1998.2	(0, 3, 9)	5178.6	
(0, 0, 5)	1998.5		(0, 8, 2)	5193.6	5214
(0, 3, 1)	2078.2	2081.7	(1, 4, 4)	5217.6	
(0, 1, 4)	2158.2		(0, 1, 12)	5224.9	
(0, 4, 0)	2232.4	2236.2	(2, 0, 6)	5231.3	
(1, 0, 2)	2247.0		(1, 7, 0)	5266.0	
(0, 2, 3)	2317.5		(0, 6, 5)	5273.0	
(0, 0, 6)	2390.6		(2, 3, 2)	5276.1	
(1, 1, 1)	2398.5	2400.3	(3, 2, 0)	5288.9	
(0, 3, 2)	2474.8	2482.7	(1, 2, 7)	5299.6	
(1, 2, 0)	2549.2		(0, 4, 8)	5339.2	
(0, 1, 5)	2550.8		(0, 9, 1)	5343.4	5363.5
(0, 4, 1)	2629.8	2634.1	(1, 5, 3)	5366.1	
(1, 0, 3)	2646.6		(1, 0, 10)	5371.0	
(0, 2, 4)	2710.7		(2, 1, 5)	5378.2	
(0, 0, 7)	2780.0		(0, 2, 11)	5390.9	
(0, 5, 0)	2782.3	2788.9	(3, 0, 3)	5411.2	
(1, 1, 2)	2798.8	2799.4	(2, 4, 1)	5418.3	
(2, 0, 0)	2840.4	2843.8	(0, 7, 4)	5427.0	
(0, 3, 3)	2868.8		(0, 0, 14)	5431.1	
(0, 1, 6)	2940.8		(1, 3, 6)	5452.4	
(1, 2, 1)	2950.2	2950.2	(0, 10, 0)	5491.4	5505.5
(0, 4, 2)	3024.6	3034.7	(0, 5, 7)	5497.7	
(1, 0, 4)	3043.7		(1, 6, 2)	5512.7	5522.2
(1, 3, 0)	3099.5	3096.8	(2, 2, 4)	5524.6	
(0, 2, 5)	3101.4		(1, 1, 9)	5526.5	
(0, 0, 8)	3166.8		(4, 0, 0)	5534.9	
(0, 5, 1)	3178.0	3185.8	(3, 1, 2)	5551.2	
(1, 1, 3)	3196.4		(0, 3, 10)	5554.7	
(2, 0, 1)	3245.4		(2, 5, 0)	5557.8	
(0, 3, 4)	3260.2		(0, 8, 3)	5579.1	
(0, 1, 7)	3328.3		(0, 1, 13)	5596.6	
(0, 6, 0)	3329.1	3337.6	(1, 4, 5)	5603.6	
(1, 2, 2)	3348.4	3351.7	(2, 0, 7)	5620.9	
(2, 1, 0)	3390.1		(0, 6, 6)	5654.3	

Table 3: Continued.

(n_1, n_2, n_3)	This work	Expt. [13]	(n_1, n_2, n_3)	This work	Expt. [13]
(0, 4, 3)	3416.8		(1, 7, 1)	5657.5	
(1, 0, 5)	3438.4		(2, 3, 3)	5669.3	
(0, 2, 6)	3489.5		(1, 2, 8)	5681.5	
(1, 3, 1)	3498.5	3497.9	(3, 2, 1)	5689.9	
(0, 0, 9)	3550.8		(0, 4, 9)	5716.2	
(0, 5, 2)	3571.1	3583.3	(0, 9, 2)	5729.9	5753.4
(1, 1, 4)	3591.4		(1, 0, 11)	5748.6	
(1, 4, 0)	3646.2	3646.9	(1, 5, 4)	5752.8	
(2, 0, 2)	3647.6		(0, 2, 12)	5763.8	
(0, 3, 5)	3649.0		(2, 1, 6)	5768.1	
(0, 1, 8)	3713.1		(1, 8, 0)	5800.3	
(0, 6, 1)	3723.1	3734.1	(0, 0, 15)	5802.6	
(1, 2, 3)	3744.0		(3, 0, 4)	5808.4	
(2, 1, 1)	3793.0		(0, 7, 5)	5808.9	
(0, 4, 4)	3806.4		(2, 4, 2)	5812.3	
(1, 0, 6)	3830.5		(3, 3, 0)	5826.3	
(0, 7, 0)	3873.1	3885.2	(1, 3, 7)	5834.9	
(0, 2, 7)	3875.0		(0, 5, 8)	5875.6	
(1, 3, 2)	3894.7	3894.3	(0, 10, 1)	5879.2	5899.5
(0, 0, 10)	3931.9		(1, 6, 3)	5900.3	
(2, 2, 0)	3937.5		(1, 1, 10)	5904.6	
(0, 5, 3)	3961.5		(2, 2, 5)	5914.8	
(1, 1, 5)	3983.8		(0, 3, 11)	5928.5	
(0, 3, 6)	4035.2		(4, 0, 1)	5939.1	
(1, 4, 1)	4043.3		(3, 1, 3)	5949.2	
(2, 0, 3)	4047.3		(2, 5, 1)	5952.8	
(0, 1, 9)	4095.1		(0, 8, 4)	5962.3	
(0, 6, 2)	4114.5	4131.2	(0, 1, 14)	5967.2	
(1, 2, 4)	4136.9		(1, 4, 6)	5986.7	
(1, 5, 0)	4189.3	4194.7	(2, 0, 8)	6007.6	
(2, 1, 2)	4193.0		(0, 11, 0)	6026.6	6040.2
(0, 4, 5)	4193.5		(0, 6, 7)	6033.0	
(3, 0, 0)	4204.5		(1, 7, 2)	6046.0	6058.04
(1, 0, 7)	4219.9		(2, 3, 4)	6060.0	
(0, 2, 8)	4257.9		(1, 2, 9)	6060.3	
(0, 7, 1)	4265.5	4279.1	(4, 1, 0)	6071.0	
(1, 3, 3)	4288.2		(3, 2, 2)	6088.4	
(0, 0, 11)	4310.4		(2, 6, 0)	6090.7	
(2, 2, 1)	4338.4		(0, 4, 10)	6091.0	
(0, 5, 4)	4349.4		(0, 9, 3)	6113.9	
(1, 1, 6)	4373.7		(1, 0, 12)	6122.9	
(0, 8, 0)	4414.6	4226.2	(0, 2, 13)	6135.4	
(0, 3, 7)	4418.9		(1, 5, 5)	6136.7	
(1, 4, 2)	4437.4	4442.1	(2, 1, 7)	6155.4	
(2, 0, 4)	4444.4		(0, 0, 16)	6177.2	
(0, 1, 10)	4474.4		(0, 7, 6)	6188.6	
(2, 3, 0)	4481.3		(1, 8, 1)	6190.1	
(0, 6, 3)	4503.2		(3, 0, 5)	6203.0	
(1, 2, 5)	4527.1		(2, 4, 3)	6203.3	
(0, 4, 6)	4577.8		(1, 3, 8)	6214.4	
(1, 5, 1)	4584.4		(3, 3, 1)	6225.4	
(2, 1, 3)	4590.7		(0, 5, 9)	6251.1	

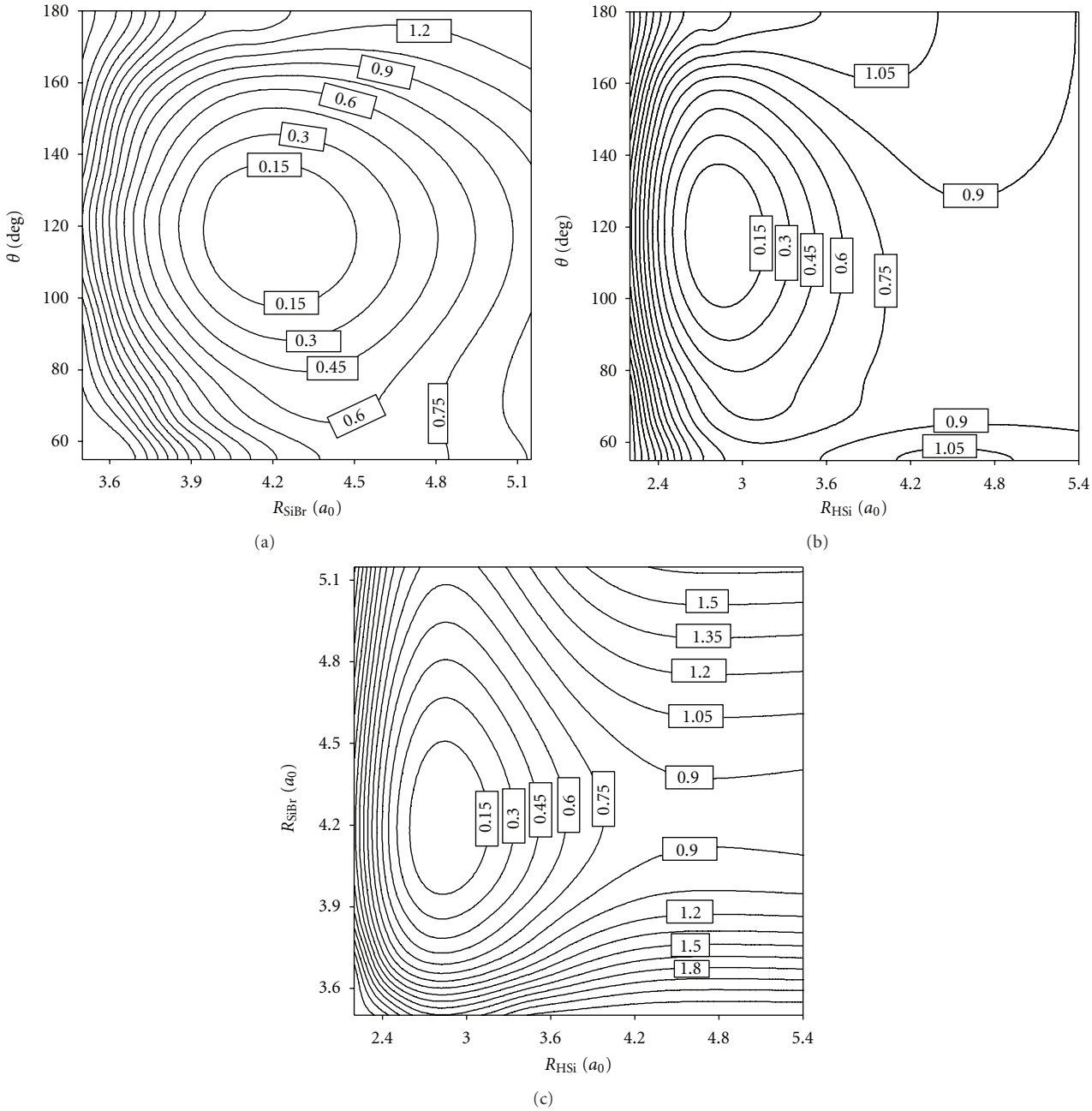

Figure 3: Contour plots of the potential energy surface of HSiBr ($\widetilde{A}^1A''$) in the internal coordinates. (a) Contour plot at $R_{HSi} = 2.833\,a_0$. (b) Contour plot at $R_{SiBr} = 4.193\,a_0$. (c) Contour plot at θ=117.7°. Contours are spaced by 0.15 eV with the zero defined at the HSiBr($\widetilde{A}^1A''$) minimum.

Davidson correction for higher excitations (MRCI + Q), respectively, employing an augmented correlation-consistent polarized valence quadruple zeta (AVQZ) basis set. The vibrational energy levels on both the two electronic states as well as the absorption and emission spectra were calculated and compared with the available experimental data. The reasonable good agreement between our results and experimental data demonstrates that the PESs are very accurate. This paper is organized as follows. In Section 2, we describe the details of the *ab initio* calculations and the analytical representation of the PESs and transition dipole moments, as well as the quantum mechanical method to calculate the vibrational energy levers. Section 3 discusses the main features of the PESs, vibrational states, and electronic spectra, respectively. A brief conclusion is summarized in Section 4.

2. Computational Details

2.1. Potential Energy Surfaces and Transition Dipole Moment Surface. Ab initio calculations were carried out to determine the potential energy surfaces (PESs) for both the $\widetilde{X}^1A'$ and

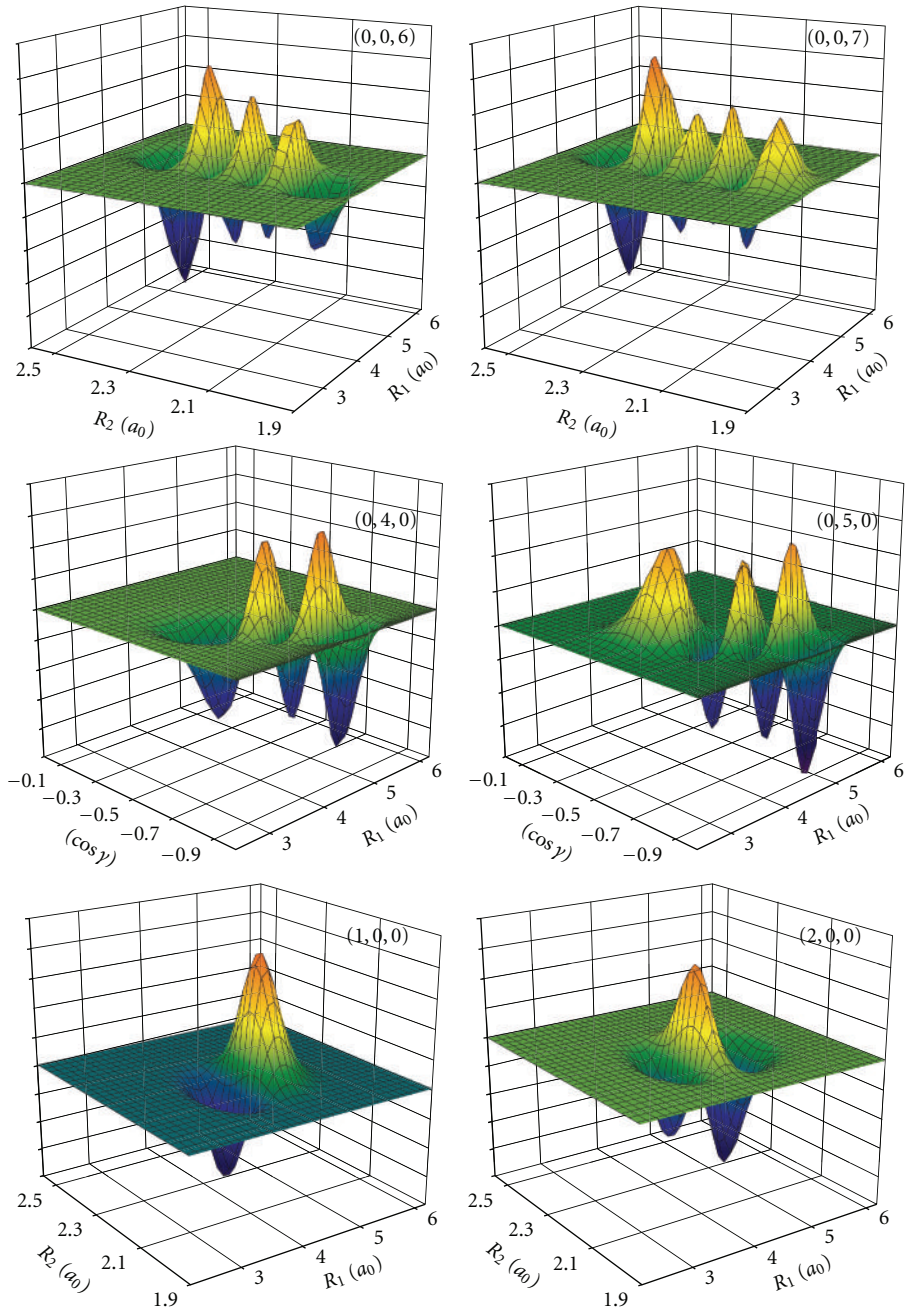

Figure 4: Six vibrational wave functions of HSiBr ($\tilde{A}^1A''$) in the Radau coordinates. The three vibrational quantum numbers (n_1, n_2, n_3) represent the H–Si stretching, bending, and Si–Br stretching modes, respectively.

$\tilde{A}^1A''$ states of HSiBr by using the MOLPRO [21] suite of quantum chemistry programs. The corresponding transition dipole moment surfaces were also calculated in this work.

The two PESs were constructed independently. For the closed-shell ground ($\tilde{X}^1A'$) electronic state, the single-reference RCCSD(T) method [22] was employed with Dunning's AVQZ basis set [23], which generates a total of 223 cGTOs, and the core electrons were frozen in all the *ab initio* calculations. A nonuniform and truncated direct product grid in the internal coordinates ($R_{\mathrm{HSi}}, R_{\mathrm{SiBr}}, \theta$) was selected for the calculations of PES, where R_{HSi} and R_{SiBr} are the H–Si and Si–Br internuclear distances, respectively, and θ is the enclosed bond angle $\angle$HSiBr. For the two radial coordinates, we have chosen 17 points covering the H–Si radial coordinate from $2.2\,a_0$ to $6.5\,a_0$ and 15 points in the Si–Br radial coordinate from $3.2\,a_0$ to $5.4\,a_0$. In the angle coordinate, 12 points ranging from 55° to 180° were used. This gives a total of 3060 geometry-unique points.

In the case of the open-shell excited electronic state ($\tilde{A}^1A''$) of HSiBr, which can not be adequately treated

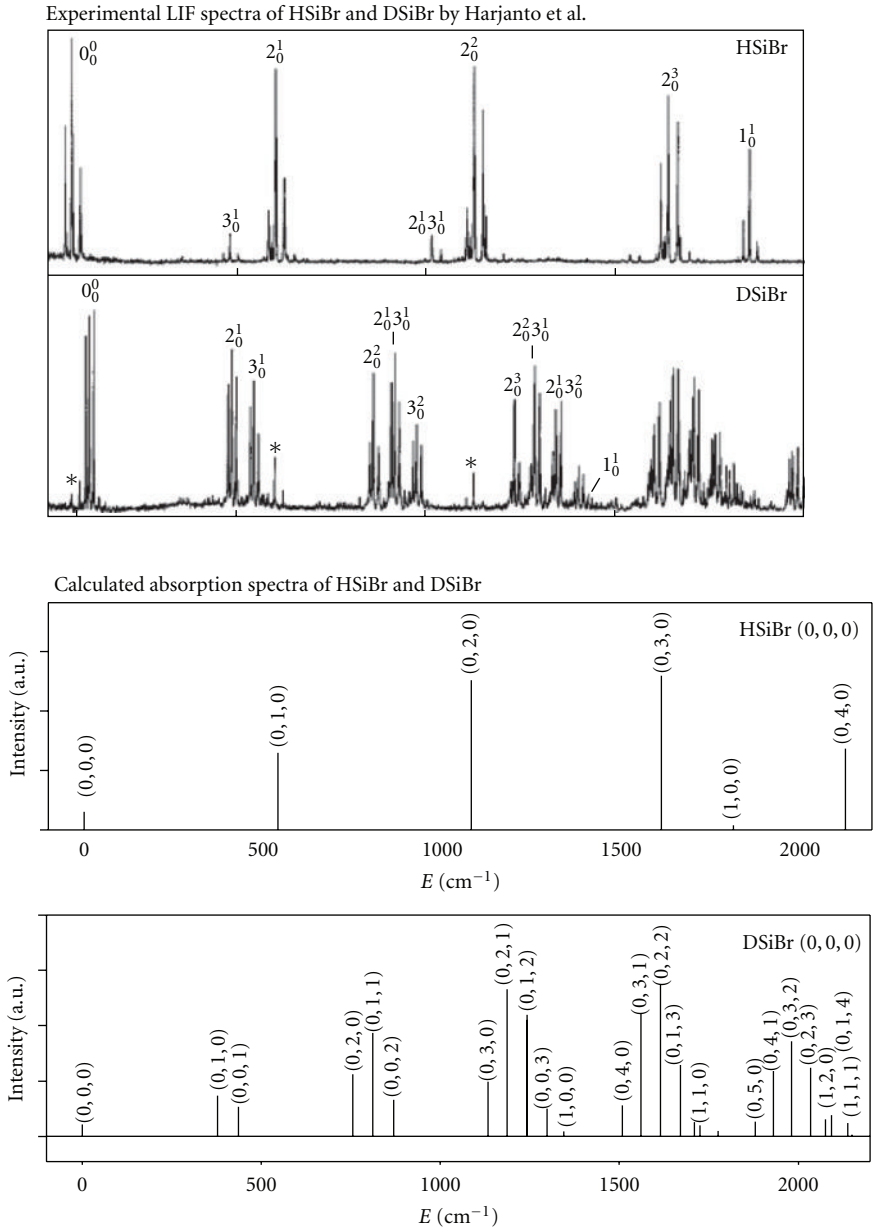

Figure 5: Calculated stick absorption spectra for the $\widetilde{A}^1A'' \leftarrow \widetilde{X}^1A'$ transition from the lowest vibrational level $\widetilde{X}(0, 0, 0)$ of HSiBr and DSiBr with the corresponding portion of the experimental LIF spectrum [8] (on the top of the calculated ones), respectively.

by single electronic configuration, the MRCI + Q [24–26] calculations were carried out using the Dunning's AVQZ basis set. After primary test calculations, the state-averaged complete active space self-consistent field (SA-CASSCF) [27, 28] for equally weighted $1^1A''$ and $2^1A''$ states were employed with a large active space (18 active electrons in 12 active orbitals) to further consider the core-valence correlation effect [15, 18–20]. The remnant sixteen core orbitals were kept doubly occupied but fully optimized. Based on the CASSCF natural orbitals, the subsequent MRCI + Q calculations were carried out for the full valence active space (12 electrons in 9 orbitals), where core-valence and core-core correlations were also included by single and double excitations from three $2p$ orbitals of Si in each configuration state function. The total number of contracted configurations is about 8.3×10^8. A relatively extensive range is also chosen for the *ab initio* points. In particular, sixteen points from 2.2 to $5.5\,a_0$ for R_{HSi} and fourteen points from 3.25 to $5.15\,a_0$ for R_{SiBr} were selected. In the angle direction, twelve points were used ranging from 55 to 180°. A total of 2688 geometry-unique points were generated.

In addition, we have also calculated the non-zero $(\widetilde{A}^1A'' - \widetilde{X}^1A')$ transition dipole moment, which is perpendicular to the molecular plane, using the MRCI + Q method with the AVTZ basis set.

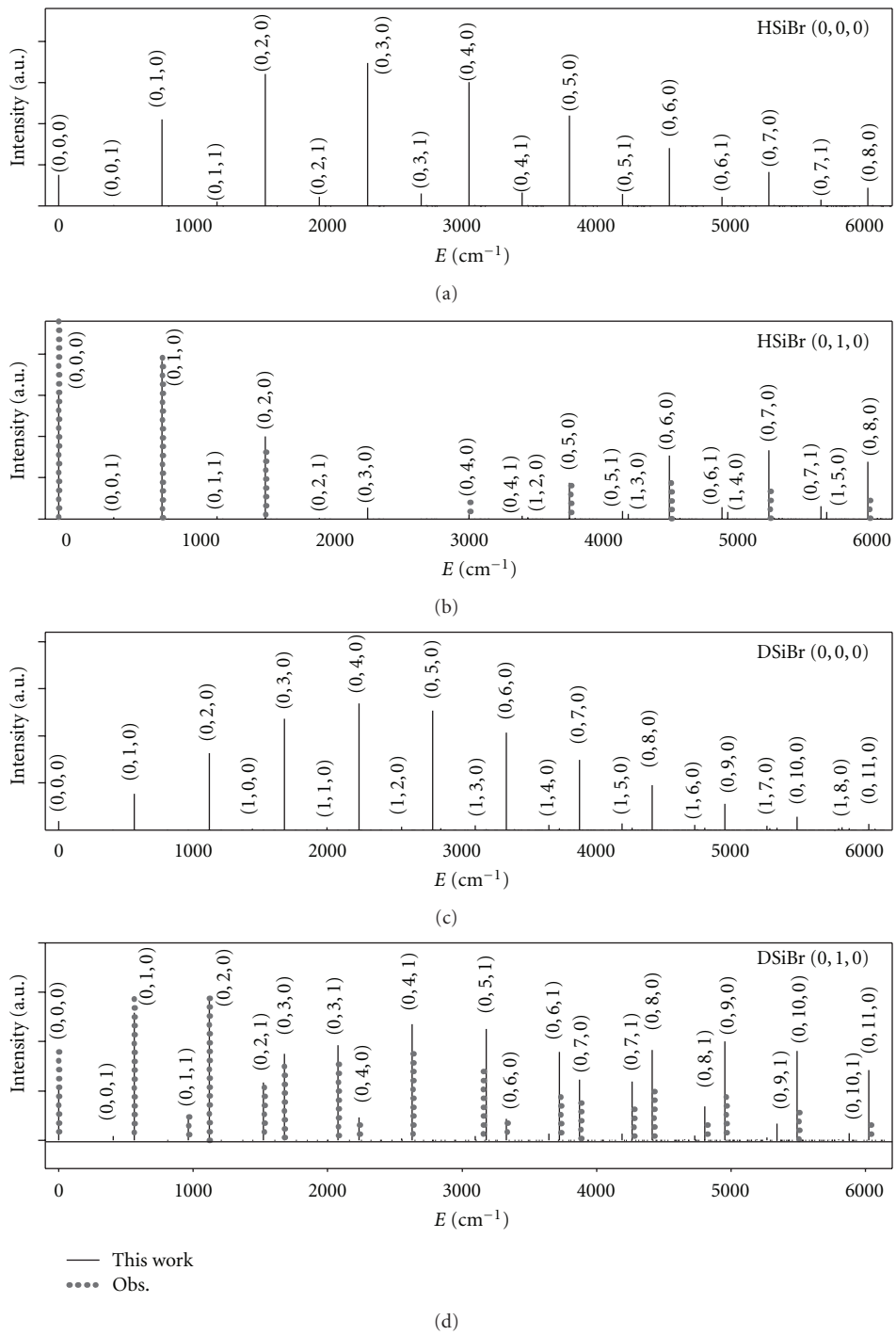

Figure 6: Calculated stick emission spectra for the $\widetilde{A}^1A'' \rightarrow \widetilde{X}^1A'$ transition from $(0,0,0)$ and $(0,1,0)$ vibrational levels of HSiBr and DSiBr. The experimental spectra were taken from [13].

Finally, the potential energies and the transition dipole moment at any arbitrary point were obtained using the three-dimensional cubic spline interpolation. The corresponding FORTRAN codes are available upon request.

2.2. Vibrational Energy Levels. The vibrational energy levels were obtained by solving the vibrational Hamiltonian with the total angular momentum $J = 0$ in Radau coordinates (R_1, R_2, γ),

$$\hat{H} = -\frac{\hbar^2}{2m_1}\frac{\partial^2}{\partial R_1^2} - \frac{\hbar^2}{2m_2}\frac{\partial^2}{\partial R_2^2} - \frac{\hbar^2}{2}\left(\frac{1}{m_1R_1^2} + \frac{1}{m_2R_2^2}\right)\left(\frac{\partial^2}{\partial\gamma^2} + \cot\gamma\frac{\partial}{\partial\gamma}\right) + V(R_1, R_2, \gamma), \quad (1)$$

Table 3: Continued.

(n_1, n_2, n_3)	This work	Expt. [13]	(n_1, n_2, n_3)	This work	Expt. [13]
(1, 0, 8)	4606.5		(0, 10, 2)	6264.2	6286.9
(3, 0, 1)	4609.4		(1, 1, 11)	6279.5	
(0, 2, 9)	4638.2		(1, 6, 4)	6285.0	
(0, 7, 2)	4655.2	4673.4	(0, 3, 12)	6300.5	
(1, 3, 4)	4679.0		(2, 2, 6)	6302.5	
(0, 0, 12)	4686.2		(1, 9, 0)	6332.2	
(1, 6, 0)	4729.1	4736.7	(0, 1, 15)	6339.0	
(0, 5, 5)	4734.6		(4, 0, 2)	6339.4	
(2, 2, 2)	4736.4		(0, 8, 5)	6342.3	
(3, 1, 0)	4747.9		(2, 5, 2)	6344.9	
(1, 1, 7)	4760.8		(3, 1, 4)	6346.0	
(0, 3, 8)	4800.0		(3, 4, 0)	6359.9	
(0, 8, 1)	4805.5	4824	(1, 4, 7)	6366.9	
(1, 4, 3)	4828.9		(2, 0, 9)	6391.5	
(2, 0, 5)	4839.1		(0, 6, 8)	6409.3	
(0, 1, 11)	4851.0		(0, 11, 1)	6412.8	6433.9
(2, 3, 1)	4880.2		(1, 7, 3)	6431.7	
(0, 6, 4)	4889.5		(1, 2, 10)	6435.9	
(1, 2, 6)	4914.7		(2, 3, 5)	6448.0	
(0, 9, 0)	4954.1	4966.8	(0, 4, 11)	6463.7	

where m_1 and m_2 are the atomic mass of H and Br, respectively. The transformation between the Radau coordinates (R_1, R_2, γ) and the internal coordinates (R_{HSi}, R_{SiBr}, θ) is well documented [29]. The vibrational wave functions were represented in a direct product discrete variable representation (DVR) [30] grid, and the vibrational energy levels were calculated using the Lanczos algorithm [31], which generates the eigenvalues of the Hamiltonian by a three-term recursion. Extensive convergence tests were carried out to ascertain the accuracy of the results against the number of recursion steps and grid size. When eigenfunctions were required, the Lanczos recursion was repeated to assemble the wave functions of interest.

For the ground electronic state, R_1 was represented by 50 potential optimized DVR (PODVR) [32, 33] grid points derived from the one-dimensional Hamiltonian, in which the two other coordinates were fixed at their equilibrium values. The other radial coordinate R_2 was represented by 30 PODVR grid points from the corresponding one-dimensional Hamiltonian. For the angular variable, 80 Gauss-Legendre [34] grid points were used. The converged vibrational energy levels below 7500 cm^{-1} were generated by performing about 7000 Lanczos recursion steps with a cutoff of 4.0 eV for the potential energy.

In the case of the excited electronic state of HSiBr, different parameters were used for calculating the vibrational states. The PODVR grids for R_1 and R_2 consist of 50 and 30 points, respectively. 80 Gauss-Legendre grid points in the interval $[0^\circ, 180^\circ]$ were used for γ. The converged vibrational energy levels below 6000 cm^{-1} were generated by performing about 5000 Lanczos recursion steps with a cutoff of 2.5 eV for the potential energy.

2.3. Absorption and Emission Spectra. The absorption and emission spectra can be evaluated as

$$\Sigma(\omega) \propto \left| \langle \Phi_n | \mu | \Psi_{n'} \rangle \right|^2, \tag{2}$$

where μ is the transition dipole moment and Φ_n and $\Psi_{n'}$ are the vibrational wave functions of the ground and excited electronic states, respectively. The transition amplitude $\langle \Phi_n | \mu | \Psi_{n'} \rangle$ can be calculated directly from the vibrational wave functions, but, in this work, we have used an efficient single Lanczos propagation (SLP) method [35, 36]. This method is particularly efficient for calculating emission from multiple excited state levels, because it requires no explicit construction and storage of the vibrational wave functions, and it has been proved successful in a number of systems [37].

For the calculation of electronic spectra, the Hamiltonians for both the ground and excited electronic states need to be represented by the same DVR grid. For both absorption and emission spectra, 60 sine-DVR points were employed to cover the R_1 range of [2.10, 8.00] a_0 and 40 sine-DVR points for the R_2 range of [1.7, 2.7] a_0. For γ, an eighty-point Gauss-Legendre DVR grid was used.

3. Results and Discussions

3.1. Ground ($\tilde{X}^1A'$) State Potential and Vibrational Energy Levels. Figure 1 displays the contour plots of the ground electronic state PES of HSiBr in the internal coordinates (R_{HSi}, R_{SiBr}, θ). Figures 1(a), 1(b), and 1(c) show the dependence of the potential on R_{SiBr} and θ with R_{HSi} fixed at its equilibrium value of 2.869 a_0, on R_{HSi} and θ with R_{SiBr} fixed at its equilibrium value of 4.257 a_0, and on the two bond

Table 4: Calculated vibrational energy levels (in cm^{-1}) and comparison with available experimental results for $HSi^{79}Br$ ($\widetilde{A}^1A''$).

(n_1, n_2, n_3)	This work	Expt. [8]	(n_1, n_2, n_3)	This work	Expt. [8]
(0, 0, 0)	0.0		(0, 7, 0)	3471.9	
(0, 0, 1)	416.5	416.54	(0, 2, 6)	3497.2	
(0, 1, 0)	541.8	535.31	(1, 1, 3)	3546.3	
(0, 0, 2)	828.8		(0, 0, 9)	3590.8	
(0, 1, 1)	956.6	949.37	(0, 3, 5)	3619.6	
(0, 2, 0)	1081.1	1059.20	(1, 2, 2)	3634.3	
(0, 0, 3)	1237.5		(1, 3, 1)	3710.8	3641.02
(0, 1, 2)	1367.1		(0, 4, 4)	3724.3	
(0, 2, 1)	1492.9	1470.89	(0, 1, 8)	3742.1	
(0, 3, 0)	1613.0	1569.07	(1, 4, 0)	3766.1	3675.59
(0, 0, 4)	1642.7		(0, 5, 3)	3806.0	
(0, 1, 3)	1774.4		(0, 6, 2)	3841.9	
(1, 0, 0)	1813.7	1786.96	(2, 0, 1)	3842.1	3784.87
(0, 2, 2)	1900.2		(1, 0, 5)	3846.1	
(0, 3, 1)	2021.1	1977.88	(0, 7, 1)	3872.3	
(0, 0, 5)	2043.6		(0, 2, 7)	3883.8	
(0, 4, 0)	2126.6	2060.57	(2, 1, 0)	3894.6	3828.00
(0, 1, 4)	2178.3		(1, 1, 4)	3947.3	
(1, 0, 1)	2227.7	2200.77	(0, 0, 10)	3963.8	
(0, 2, 3)	2304.8		(0, 3, 6)	4009.5	
(1, 1, 0)	2321.3	2286.15	(1, 2, 3)	4036.3	
(0, 3, 2)	2424.6		(0, 9, 0)	4076.1	
(0, 0, 6)	2439.2		(1, 3, 2)	4112.0	
(0, 4, 1)	2531.4		(0, 1, 9)	4119.3	
(0, 1, 5)	2577.7		(1, 4, 1)	4165.5	
(0, 5, 0)	2614.0	2526.79	(1, 5, 0)	4196.8	4069.35
(1, 0, 2)	2637.7		(1, 0, 6)	4240.2	
(0, 2, 4)	2706.7		(2, 0, 2)	4247.4	
(1, 1, 1)	2733.5	2697.66	(0, 2, 8)	4264.0	
(1, 2, 0)	2819.9	2770.59	(2, 1, 1)	4299.7	4229.06
(0, 3, 3)	2825.4		(0, 0, 11)	4331.9	
(0, 0, 7)	2829.2		(2, 2, 0)	4339.7	4261.83
(0, 4, 2)	2931.4		(1, 1, 5)	4344.0	
(0, 1, 6)	2971.8		(0, 10, 0)	4359.5	
(0, 5, 1)	3015.5		(0, 3, 7)	4393.4	
(1, 0, 3)	3044.0		(1, 2, 4)	4434.8	
(0, 6, 0)	3065.2		(0, 9, 1)	4481.3	
(0, 2, 5)	3104.6		(0, 1, 10)	4487.9	
(1, 1, 2)	3141.7		(1, 3, 3)	4510.3	
(0, 0, 8)	3212.6		(1, 0, 7)	4628.7	
(0, 3, 4)	3224.6		(0, 2, 9)	4637.9	
(1, 2, 1)	3229.2	3179.44	(2, 0, 3)	4649.2	
(1, 3, 0)	3305.3	3235.83	(0, 0, 12)	4695.3	
(0, 4, 3)	3328.9		(2, 1, 2)	4700.6	4681.50
(0, 1, 7)	3360.0		(2, 2, 1)	4734.1	4645.25
(0, 5, 2)	3412.1		(1, 1, 6)	4735.8	
(2, 0, 0)	3432.9		(2, 3, 0)	4766.4	4620.91
(1, 0, 4)	3447.0		(0, 3, 8)	4770.9	
(0, 6, 1)	3448.6		(3, 0, 0)	4797.7	

Table 5: Calculated vibrational energy levels (in cm^{-1}) and comparison with available experimental results for $HSi^{81}Br$ ($\tilde{A}^1A''$).

(n_1, n_2, n_3)	This work	Expt. [8]	(n_1, n_2, n_3)	This work	Expt. [8]
(0, 0, 0)	0.0		(0, 7, 0)	3471.2	
(0, 0, 1)	415.1	415.23	(0, 2, 6)	3489.5	
(0, 1, 0)	541.8	535.31	(1, 1, 3)	3542.3	
(0, 0, 2)	826.1		(0, 0, 9)	3579.7	
(0, 1, 1)	955.2	947.95	(0, 3, 5)	3613.0	
(0, 2, 0)	1081.0	1059.20	(1, 2, 2)	3631.6	
(0, 0, 3)	1233.5		(1, 3, 1)	3709.4	3639.63
(0, 1, 2)	1364.4		(0, 4, 4)	3718.9	
(0, 2, 1)	1491.4	1469.44	(0, 1, 8)	3732.2	
(0, 3, 0)	1612.8	1569.07	(1, 4, 0)	3765.7	3675.25
(0, 0, 4)	1637.4		(0, 5, 3)	3801.9	
(0, 1, 3)	1770.3		(0, 6, 2)	3839.6	
(1, 0, 0)	1813.7	1786.96	(2, 0, 1)	3839.8	3783.65
(0, 2, 2)	1897.4		(1, 0, 5)	3840.8	
(0, 3, 1)	2019.6	1976.42	(0, 7, 1)	3870.7	
(0, 0, 5)	2037.1		(0, 2, 7)	3874.9	
(0, 4, 0)	2126.4	2060.57	(2, 1, 0)	3894.4	3828.00
(0, 1, 4)	2173.0		(1, 1, 4)	3942.1	
(1, 0, 1)	2226.4	2199.43	(0, 0, 10)	3951.7	
(0, 2, 3)	2300.7		(0, 3, 6)	4001.8	
(1, 1, 0)	2321.2	2286.15	(1, 2, 3)	4032.3	
(0, 3, 2)	2421.8		(0, 9, 0)	4075.0	
(0, 0, 6)	2431.5		(1, 3, 2)	4105.7	
(0, 4, 1)	2529.9		(0, 1, 9)	4110.7	
(0, 1, 5)	2571.2		(1, 4, 1)	4164.2	
(0, 5, 0)	2613.8	2526.79	(1, 5, 0)	4192.3	4068.67
(1, 0, 2)	2635.0		(1, 0, 6)	4232.6	
(0, 2, 4)	2701.4		(2, 0, 2)	4245.0	
(1, 1, 1)	2732.1	2696.27	(0, 2, 8)	4254.1	
(1, 2, 0)	2819.5	2770.59	(2, 1, 1)	4298.5	4228.03
(0, 3, 3)	2819.8		(0, 0, 11)	4318.7	
(0, 0, 7)	2822.1		(2, 2, 0)	4337.6	4261.15
(0, 4, 2)	2928.6		(1, 1, 5)	4339.3	
(0, 1, 6)	2964.1		(0, 10, 0)	4357.6	
(0, 5, 1)	3014.0		(0, 3, 7)	4384.6	
(1, 0, 3)	3040.1		(1, 2, 4)	4429.7	
(0, 6, 0)	3065.0		(0, 9, 1)	4475.9	
(0, 2, 5)	3098.1		(0, 1, 10)	4479.5	
(1, 1, 2)	3139.0		(1, 3, 3)	4506.4	
(0, 0, 8)	3202.6		(1, 0, 7)	4620.7	
(0, 3, 4)	3219.2		(0, 2, 9)	4631.5	
(1, 2, 1)	3227.8	3177.99	(2, 0, 3)	4645.6	
(1, 3, 0)	3305.2	3235.83	(0, 0, 12)	4681.2	
(0, 4, 3)	3324.8		(2, 1, 2)	4698.3	4620.59
(0, 1, 7)	3351.1		(2, 2, 1)	4728.2	4643.80
(0, 5, 2)	3409.3		(1, 1, 6)	4733.0	
(2, 0, 0)	3432.9		(2, 3, 0)	4761.0	4679.78
(1, 0, 4)	3441.8		(0, 3, 8)	4765.2	
(0, 6, 1)	3447.7		(3, 0, 0)	4797.7	

Table 6: Calculated vibrational energy levels (in cm^{-1}) and comparison with available experimental results for $DSi^{79}Br$ ($\widetilde{A}^1A''$).

(n_1, n_2, n_3)	This work	Expt. [8]	(n_1, n_2, n_3)	This work	Expt. [8]
(0, 0, 0)	0.0	0.00	(0,9,0)	3320.2	
(0, 1, 0)	377.8	376.41	(0,1,7)	3333.7	
(0, 0, 1)	436.3	434.34	(1,2,3)	3336.5	3291.73
(0, 2, 0)	755.7	750.48	(0,8,1)	3351.9	
(0, 1, 1)	811.7	806.10	(2,1,1)	3367.4	
(0, 0, 2)	869.0	864.77	(0,7,2)	3391.1	
(0, 3, 0)	1133.0	1121.95	(1,1,4)	3398.8	
(0, 2, 1)	1187.1	1174.58	(0,0,8)	3411.2	
(0, 1, 2)	1243.0	1231.27	(0,6,3)	3436.6	
(0, 0, 3)	1298.7	1290.48	(2,0,2)	3444.3	
(1, 0, 0)	1344.7	1325.55	(1,0,5)	3467.4	
(0, 4, 0)	1508.1	1490.30	(0,5,4)	3487.2	
(0, 3, 1)	1560.6	1540.58	(1,6,0)	3505.6	3436.43
(0, 2, 2)	1614.5	1594.60	(0,4,5)	3541.7	
(0, 1, 3)	1670.4	1651.70	(1,5,1)	3560.7	3498.71
(1, 1, 0)	1710.6	1688.70	(0,3,6)	3600.2	
(0, 0, 4)	1725.9	1711.77	(1,4,2)	3619.1	3562.48
(1, 0, 1)	1775.9	1754.76	(2,3,0)	3637.3	3579.61
(0, 5, 0)	1879.8	1855.22	(0,10,0)	3639.9	
(0, 4, 1)	1930.6	1902.26	(0,2,7)	3665.9	
(0, 3, 2)	1982.5	1953.86	(1,3,3)	3680.7	3628.07
(0, 2, 3)	2036.6	2008.99	(0,9,1)	3682.0	
(1, 2, 0)	2075.8	2048.42	(2,2,1)	3710.5	3659.77
(0, 1, 4)	2093.2	2067.22	(0,8,2)	3721.3	
(1, 1, 1)	2138.0	2112.79	(0,1,8)	3739.9	
(0, 0, 5)	2151.5		(1,2,4)	3743.4	
(1, 0, 2)	2203.3	2180.27	(3,0,0)	3744.8	
(0, 6, 0)	2247.6	2215.53	(0,7,3)	3763.4	
(0, 5, 1)	2295.8	2259.58	(2,1,2)	3785.2	
(0, 4, 2)	2345.3	2308.59	(0,6,4)	3810.7	
(0, 3, 3)	2397.7	2361.47	(1,1,5)	3811.2	
(1, 3, 0)	2439.7	2404.43	(0,0,9)	3821.2	
(0, 2, 4)	2452.7	2418.10	(1,7,0)	3845.6	
(1, 2, 1)	2499.6	2467.46	(0,5,5)	3863.0	
(0, 1, 5)	2511.6		(2,0,3)	3863.8	
(1, 1, 2)	2562.1	2533.19	(1,0,6)	3883.8	
(0, 0, 6)	2575.1		(1,6,1)	3899.5	
(2, 0, 0)	2596.0		(0,4,6)	3925.6	
(0, 7, 0)	2611.0	2569.98	(1,5,2)	3958.2	
(1, 0, 3)	2627.3	2601.43	(2,4,0)	3975.7	3905.52
(0, 6, 1)	2655.6	2610.98	(0,3,7)	3983.0	
(0, 5, 2)	2701.8	2657.51	(1,4,3)	4019.3	
(0, 4, 3)	2752.3		(2,3,1)	4049.0	3987.77
(1, 4, 0)	2800.5	2755.51	(0,2,8)	4059.3	
(0, 3, 4)	2805.8		(3,1,0)	4070.9	
(1, 3, 1)	2858.5	2817.20	(1,3,4)	4082.4	
(0, 2, 5)	2862.9		(2,2,2)	4126.0	
(1, 2, 2)	2919.2	2881.69	(1,2,5)	4148.9	
(0, 1, 6)	2926.0		(3,0,1)	4164.5	
(2, 1, 0)	2945.8		(2,1,3)	4199.2	

Table 6: Continued.

(n_1, n_2, n_3)	This work	Expt. [8]	(n_1, n_2, n_3)	This work	Expt. [8]
(0, 8, 0)	2969.5	2912.85	(1,1,6)	4218.7	
(1, 1, 3)	2982.6	2948.95	(0,0,10)	4224.0	
(0, 0, 7)	2995.4		(1,8,0)	4229.4	
(0, 7, 1)	3008.8		(2,0,4)	4278.5	
(2, 0, 1)	3022.2		(1,7,1)	4287.6	
(1, 0, 4)	3048.5	2999.16	(1,0,7)	4296.8	
(0, 6, 2)	3051.0	3018.34	(2,5,0)	4305.2	4220.97
(0, 5, 3)	3099.2		(1,6,2)	4348.7	
(0, 4, 4)	3151.3		(2,4,1)	4380.0	4306.79
(1, 5, 0)	3156.5	3100.27	(3,2,0)	4395.1	
(0, 3, 5)	3206.7		(1,5,3)	4412.0	
(1, 4, 1)	3212.9	3161.61	(2,3,2)	4455.8	
(0, 2, 6)	3267.2		(3,1,1)	4486.9	
(1, 3, 2)	3272.4	3225.27	(3,0,2)	4581.6	
(2, 2, 0)	3293.1		(4,0,0)	4763.6	

lengths with the bond angle fixed at its equilibrium value of 93.9°, respectively. The equilibrium geometry of HSiBr at the ground electronic state PES was found to be located at $R_{\mathrm{HSi}} = 2.869\,a_0$, $R_{\mathrm{SiBr}} = 4.257\,a_0$, and $\theta = 93.9°$,which is very similar to that of HSiCl [20], except that the Si–Br bond is longer than the Si–Cl bond. Our results are compared in Table 1 with the previous experimental and theoretical results. It is clear that our equilibrium geometry is in good agreement with the experimental and theoretical values [3, 8, 13].

The calculated vibrational levels for the ground electronic state $(\widetilde{X}^1A')$ of HSiBr up to 7300 cm^{-1} are listed in Table 2, together with the available experimental values. The vibrational energy levels are assigned with three vibrational quantum numbers $(n_1,\ n_2,\ n_3)$, representing the H–Si stretching, bending, and Si–Br stretching vibrational modes, respectively. By inspecting the nodal structures of the corresponding wave functions, the assignment of the vibrational levels can be achieved. The plots of nine wave functions of HSiBr are given in Figure 2, in which the nodal structures are clearly visible. The ease of the assignment suggests that the vibration of HSiBr is largely regular with weak intramodal coupling in this spectral region.

From Table 2, it is apparent that the calculated vibrational energy levels reproduce the available experimental data very well. The fundamental frequencies of $\nu_1 = 1977.6\,\mathrm{cm}^{-1}$, $\nu_2 = 770.3\,\mathrm{cm}^{-1}$, and $\nu_3 = 409.3\,\mathrm{cm}^{-1}$ are in excellent agreement with the experimental values [13] of 1976.2, 772.0, and 412.4 cm^{-1}, respectively. The good theory-experiment agreement is held all the way to the highest experimentally assigned level (1, 7, 0) near 7200 cm^{-1}.

The vibrational energy levels of DSiBr have also been obtained on the same *ab initio* ground electronic state PES. The calculated vibrational levels up to 6500 cm^{-1} are compared with the available experimental data in Table 3. As expected, the substitution by the more massive deuterium not only lowers the energies of the H–Si stretching and bending vibrations, but also decreases the Si–Br stretching vibrational frequency to a small extent. Again, the calculated results are in excellent agreement with experiment. The calculated fundamental vibrational frequencies for the D–Si stretching, Si–Br stretching, and bending modes (1439.8, 405.0, and 562.0 cm^{-1}) are very close to the experimental values [13] (1439.5, 407.99, and 561.8 cm^{-1}), respectively. As a whole, Tables 2 and 3 show that all the calculated vibrational energy levels for HSiBr/DSiBr are within a reasonable error of the observed values, demonstrating the high accuracy of our *ab initio* ground electronic state PES.

3.2. Excited $(\widetilde{A}^1A'')$ State Potential and Vibrational Energy Levels. Figure 3 displays the PES for the excited electronic state $(\widetilde{A}^1A'')$ in the HSiBr internal coordinates $(R_{\mathrm{HSi}},\ R_{\mathrm{SiBr}},\ \theta)$. The equilibrium geometry was found to be located at $R_{\mathrm{HSi}} = 2.833\,a_0$, $R_{\mathrm{SiBr}} = 4.193\,a_0$, and $\theta = 117.7°$. In comparison with the ground state, neither the H–Si nor Si–Br bond length changes significantly, but the bending angle is extended by about 20°. One can see from Table 1 that the equilibrium geometry is consonant with the experimental and previous theoretical values [3, 8, 13].

The calculated vibrational levels for the excited $(\widetilde{A}^1A'')$ electronic states of HSi^{79}Br, HSi^{81}Br, DSi^{79}Br, and DSi^{81}Br are presented in Tables 4, 5, 6, and 7, together with the available experimental results. The energies given in the tables are relative to the ground (0, 0, 0) vibrational level on this PES. Figure 4 displays six vibrational wave functions of HSiBr on the excited electronic states. The nodal structures of the wave functions are clearly shown. The theory-experiment agreement is typically very good. For example, the calculated fundamental frequencies of the H–Si stretching, Si–^{79}Br stretching, and bending modes (1813.71, 416.50, and 541.83 cm^{-1}) are in reasonably good agreement with the experimental values (1786.96, 416.54, and 535.31 cm^{-1}) [8]. As expected, the substitution by deuterium lowers the energies of the vibrational frequencies. Since the ^{79}Br/^{81}Br ratio is much smaller than D/H, the effect

Table 7: Calculated vibrational energy levels (in cm^{-1}) and comparison with available experimental results for $DSi^{81}Br$ ($\widetilde{A}^1A''$).

(n_1, n_2, n_3)	This work	Expt. [8]	(n_1, n_2, n_3)	This work	Expt. [8]
(0,0,0)	0.0		(0,9,0)	3316.96	
(0,1,0)	377.2	375.87	(0,1,7)	3328.73	
(0,0,1)	435.4	433.44	(1,2,3)	3331.48	3287.52
(0,2,0)	754.5	749.44	(0,8,1)	3347.95	
(0,1,1)	810.3	804.70	(2,1,1)	3365.97	
(0,0,2)	867.4	863.00	(0,7,2)	3385.94	
(0,3,0)	1131.1	1120.41	(1,1,4)	3394.50	
(0,2,1)	1185.2	1173.11	(0,0,8)	3404.45	
(0,1,2)	1240.9	1228.93	(0,6,3)	3430.85	
(0,0,3)	1296.2	1287.74	(2,0,2)	3442.10	
(1,0,0)	1344.7	1325.55	(1,0,5)	3462.55	
(0,4,0)	1505.5	1488.35	(0,5,4)	3480.95	
(0,3,1)	1558.1	1538.21	(1,6,0)	3503.64	3435.14
(0,2,2)	1611.8	1591.74	(0,4,5)	3535.04	
(0,1,3)	1667.5	1648.49	(1,5,1)	3557.80	3496.22
(1,1,0)	1710.2	1688.30	(0,3,6)	3593.33	
(0,0,4)	1722.6	1708.21	(1,4,2)	3615.41	3558.80
(1,0,1)	1774.9	1753.76	(2,3,0)	3636.40	3578.93
(0,5,0)	1876.7	1852.96	(0,10,0)	3638.85	
(0,4,1)	1927.5	1899.48	(0,2,7)	3658.95	
(0,3,2)	1979.2	1950.57	(1,3,3)	3676.39	3623.67
(0,2,3)	2033.1	2005.19	(0,9,1)	3677.72	
(1,2,0)	2074.9	2047.70	(2,2,1)	3708.72	3658.01
(0,1,4)	2089.5	2063.10	(0,8,2)	3715.75	
(1,1,1)	2136.6	2111.59	(0,1,8)	3732.91	
(0,0,5)	2147.3		(1,2,4)	3739.87	
(1,0,2)	2201.3	2178.17	(3,0,0)	3743.44	
(0,6,0)	2244.0	2213.29	(0,7,3)	3757.02	
(0,5,1)	2292.3	2256.47	(2,1,2)	3782.58	
(0,4,2)	2341.5	2304.82	(0,6,4)	3804.27	
(0,3,3)	2393.6	2357.25	(1,1,5)	3805.53	
(1,3,0)	2438.4	2403.33	(0,0,9)	3813.63	
(0,2,4)	2448.4	2413.45	(1,7,0)	3843.74	
(1,2,1)	2497.8	2465.64	(0,5,5)	3856.71	
(0,1,5)	2507.2		(2,0,3)	3859.58	
(1,1,2)	2559.8	2530.70	(1,0,6)	3878.06	
(0,0,6)	2570.0		(1,6,1)	3896.57	
(2,0,0)	2596.0		(0,4,6)	3919.12	
(0,7,0)	2607.0	2567.71	(1,5,2)	3954.23	
(1,0,3)	2624.4	2598.32	(2,4,0)	3974.67	3904.78
(0,6,1)	2651.7	2607.55	(0,3,7)	3976.09	
(0,5,2)	2697.5	2653.40	(1,4,3)	4014.57	
(0,4,3)	2747.7		(2,3,1)	4046.99	3985.91
(1,4,0)	2798.8	2754.28	(0,2,8)	4051.56	
(0,3,4)	2800.9		(3,1,0)	4070.65	
(1,3,1)	2856.1	2815.08	(1,3,4)	4076.68	
(0,2,5)	2857.9		(2,2,2)	4120.45	
(1,2,2)	2916.3	2878.97	(1,2,5)	4143.05	
(0,1,6)	2920.8		(3,0,1)	4163.28	
(2,1,0)	2945.5		(2,1,3)	4195.41	

Table 7: Continued.

(n_1, n_2, n_3)	This work	Expt. [8]	(n_1, n_2, n_3)	This work	Expt. [8]
(0,8,0)	2965.5	2911.19	(1,1,6)	4212.47	
(1,1,3)	2979.3	2945.37	(0,0,10)	4215.55	
(0,0,7)	2989.5		(1,8,0)	4224.77	
(0,7,1)	3004.8		(2,0,4)	4273.99	
(2,0,1)	3021.1		(1,7,1)	4283.27	
(1,0,4)	3044.6	3014.23	(1,0,7)	4290.27	
(0,6,2)	3046.3	2994.71	(2,5,0)	4304.18	4220.13
(0,5,3)	3094.0		(1,6,2)	4343.48	
(0,4,4)	3145.7		(2,4,1)	4377.84	4304.76
(1,5,0)	3154.6	3098.96	(3,2,0)	4392.57	
(0,3,5)	3200.8		(1,5,3)	4406.13	
(1,4,1)	3210.3	3159.24	(2,3,2)	4452.59	
(0,2,6)	3261.2		(3,1,1)	4485.40	
(1,3,2)	3269.0	3221.96	(3,0,2)	4579.21	
(2,2,0)	3292.5		(4,0,0)	4763.54	

of the ^{81}Br substitution on vibrational energies of HSiBr is much less pronounced.

3.3. Absorption Spectra. The $\widetilde{A}^1A'' \leftarrow \widetilde{X}^1A'$ electronic transition of HSiBr involves an electron promotion from a silicon-based nonbonding σ orbital to an unoccupied out-of-plane Si $3p$ orbital [13]. The only non-zero transition dipole is perpendicular to the molecular plane, and it varies smoothly with the three coordinates in the Franck-Condon region. As shown in Figure 5, the calculated $\widetilde{A}^1A'' \leftarrow \widetilde{X}^1A'$ absorption spectra from the lowest state $\widetilde{X}$ (0, 0, 0) of both HSiBr and DSiBr were found to contain a relatively small number of vibronic bands. The spectral positions of the vibronic bands of HSiBr and DSiBr are consistent with the experimental spectra obtained with the laser-induced fluorescence technique [8]. Since the experimental LIF spectrum may often be composed of several different fragment portions which were recorded under different experimental conditions and involve the influence of rotational structures, some observable bands cannot be reproduced in our calculations. Considering the approximately 20° change in the bending equilibrium angle, it is anticipated that the absorption is dominated by excitation in the bending mode. Indeed, the calculated absorption spectrum for HSiBr is dominated by the (0, n_2, 0) progression. On the other hand, the spectrum of DSiBr is more complex than that of HSiBr. Besides the (0, n_2, 0) progression, the (0, 0, n_3) band and some combination bands are of comparable intensities. In addition, several weaker bands such as $(1, 0, 0)$, $(1, 1, 0)$, and $(1, 1, 1)$ are visible.

3.4. Emission Spectra. The calculated $\widetilde{A}^1A'' \rightarrow \widetilde{X}^1A'$ emission spectra from the $(0, 0, 0)$ and $(0, 1, 0)$ vibrational states of the excited electronic state of HSiBr and DSiBr and the comparison with the available experimental observations are shown in Figure 6. The spectra are concentrated in the spectral region within 6000 cm^{-1} above the band origin, and it is clear that the experimental emission spectra of Hostutler et al. [13] are well reproduced by the calculated ones. As shown in this figure, the emission spectra from the vibrational state $\widetilde{A}$(0, 1, 0) of HSiBr is dominated by the (0, n_2, 0) progression. The good agreement between theory and experiment again suggests that both the ground and excited state PESs are quite reliable. Also shown in Figure 6, the calculated emission spectra from the vibrational state of $\widetilde{A}$(0, 0, 0) is also dominated by the (0, n_2, 0) progression.

The essential features of the spectra are similar for the two isotopomers, but the DSiBr spectra are more congested than that of HSiBr due to the larger mass of deuterium. One can see from Figure 6 that the emission spectrum from $\widetilde{A}$(0, 0, 0) of DSiBr is featured by the dominated (0, n_2, 0) and weaker (1, n_2, 0) progressions. The large bending excitation is due to the about 20° increase in the bond angle upon electronic excitation. In the same figure, the calculated emission spectrum from the $\widetilde{A}$(0, 1, 0) of DSiBr is compared to the experimental data of Hostutler et al. [13] As expected, the spectrum bending progressions are dominated, with 0 and 1 quanta in the Si-Br mode, respectively. The overall agreement with the experiment is very good. These emission spectra show that the spectral pattern is quite sensitive to the vibrational state from which the emission originates. These observations are very similar to those in our previous work about HSiCl [20].

4. Conclusions

In this work, we have reported accurate *ab initio* PESs for both the ground ($\widetilde{X}^1A'$) and excited electronic states ($\widetilde{A}^1A''$) of HSiBr, as well as the $\widetilde{A}^1A'' - \widetilde{X}^1A'$ transition dipole moment. By spline interpolation of numerous *ab initio* points which were obtained at high *ab initio* level of theory, the nonempirical three-dimensional potential energy surfaces and transition dipole moment function were constructed. Some low-lying vibrational energy levels of

both HSiBr and DSiBr were determined using the Lanczos recursion method. The calculated results are in good agreement with the available experimental data, demonstrating the good quality of both the ground and excited state PESs. In addition, the absorption and emission spectra of HSiBr/DSiBr were calculated using an efficient single Lanczos propagation method, and the resulting spectra were found to be fairly consistent with experimental observations. Similar to HSiCl, the approximately 20° difference in the HSiBr equilibrium bending angle in the two electronic states leads to significant bending excitations in both absorption and emission spectra. Our theoretical results reported provide necessary insight into the vibrational dynamics of the HSiBr molecule in its ground and excited electronic states.

Acknowledgments

D.X. acknowledges support from the National Natural Science Foundation of China (Grant Nos. 20725312 and 91021010), from the Ministry of Science and Technology (2007CB815201), and from the Fundamental Research Funds for the Central Universities (1114020503).

References

[1] J. M. Jasinski, B. S. Meyerson, and B. A. Scott, "Mechanistic studies of chemical vapor-deposition," *Annual Review of Physical Chemistry*, vol. 38, no. 1, pp. 109–140, 1987.

[2] S. K. Murad, S. P. Beaumont, and C. D. W. Wilkinson, "New chemistry for selective reactive ion etching of InGaAs and InP over InAlAs in $SiCl_4/SiF_4/HBr$ plasmas," *Applied Physics Letters*, vol. 67, no. 18, pp. 2660–2662, 1995.

[3] G. Herzberg and R. D. Verma, "Spectra & structures of free HSiCl & HSiBr radicals," *Canadian Journal of Physics*, vol. 42, no. 3, pp. 395–432, 1964.

[4] J. T. Hougen and J. K. G. Watson, "Anomalous rotational line intensities in electronic transitions of polyatomic molecules-axis-switching," *Canadian Journal of Physics*, vol. 43, no. 2, pp. 298–320, 1965.

[5] N. L. Shinkle and J. B. Coon, "A variable reduced mass model for quasi-linear molecules with application to HSiBr," *Journal of Molecular Spectroscopy*, vol. 40, no. 2, pp. 217–227, 1971.

[6] W. A. Gilchrist, E. Reyna, and J. B. Coon, "Geometrical structures, bending potentials, and vibrational frequencies $\nu_1$for $^1A''$ states of HSiBr, HSiCl, and DSiCl," *Journal of Molecular Spectroscopy*, vol. 74, no. 3, pp. 345–360, 1979.

[7] J. I. Steinfeld, "Reactions of photogenerated free radicals at surfaces of electronic materials," *Chemical Reviews*, vol. 89, no. 6, pp. 1291–1301, 1989.

[8] H. Harjanto, W. W. Harper, and D. J. Clouthier, "Resolution of anomalies in the geometry and vibrational frequencies of monobromosilylene (HSiBr) by pulsed discharge jet spectroscopy," *The Journal of Chemical Physics*, vol. 105, no. 23, pp. 10189–10200, 1996.

[9] W. W. Harper and D. J. Clouthier, "Reinvestigation of the HSiCl electronic spectrum: experimental reevaluation of the geometry, rotational constants, and vibrational frequencies," *The Journal of Chemical Physics*, vol. 106, no. 23, pp. 9461–9473, 1997.

[10] W. W. Harper, E. A. Ferrall, R. K. Hilliard, S. M. Stogner, R. S. Grev, and D. J. Clouthier, "Laser spectroscopic detection of the simplest unsaturated silylene and germylene," *Journal of the American Chemical Society*, vol. 119, no. 35, pp. 8361–8362, 1997.

[11] W. W. Harper, D. A. Hostutler, and D. J. Clouthier, "Pulsed discharge jet spectroscopy of DSiF and the equilibrium molecular structure of monofluorosilylene," *The Journal of Chemical Physics*, vol. 106, no. 11, pp. 4367–4375, 1997.

[12] D. A. Hostutler, D. J. Clouthier, and R. H. Judge, "Single vibronic level emission spectroscopy of jet-cooled HSiF and DSiF," *The Journal of Chemical Physics*, vol. 114, no. 24, pp. 10728–10732, 2001.

[13] D. A. Hostutler, N. Ndiege, D. J. Clouthier, and S. W. Pauls, "Emission spectroscopy, harmonic vibrational frequencies, and improved ground state structures of jet-cooled monochloro—and monobromosilylene (HSiCl and HSiBr)," *The Journal of Chemical Physics*, vol. 115, no. 12, pp. 5485–5491, 2001.

[14] B. S. Tackett and D. J. Clouthier, "Structural and spectroscopic trends in the ground states of the monohalosilylenes: emission spectroscopy of jet-cooled HSiI and DSiI," *The Journal of Chemical Physics*, vol. 118, no. 6, pp. 2612–2619, 2003.

[15] D. K. W. Mok, E. P. F. Lee, F. T. Chau, and J. M. Dyke, "Franck-Condon simulation of the single vibronic level emission spectra of HSiF and DSiF including anharmonicity," *The Journal of Chemical Physics*, vol. 120, no. 3, pp. 1292–1305, 2004.

[16] B. S. Tackett, D. J. Clouthier, J. N. Landry, and W. Jager, "Fourier transform microwave spectroscopy of HSiBr: exploring the Si-Br bond through quadrupole hyperfine coupling," *The Journal of Chemical Physics*, vol. 122, no. 21, Article ID 214314, 6 pages, 2005.

[17] D. W. K. Mok, E. P. F. Lee, F. T. Chau, and J. M. Dyke, "Franck-Condon simulations including anharmonicity of the A^1A''-X^1A' absorption and single vibronic level emission spectra of HSiCl and DSiCl," *Journal of Chemical Theory and Computation*, vol. 5, no. 3, pp. 565–579, 2009.

[18] S. Lin, D. Xie, and H. Guo, "*Ab initio* potential energy surfaces for both the ground $(X^1A')$and excited (X^1A') and excited (A^1A'') electronic states of HGeCl and the absorption and emission spectra of HGeCl/DGeCl," *The Journal of Chemical Physics*, vol. 129, no. 15, Article ID 154313, 11 pages, 2008.

[19] S. Lin, D. Xie, and H. Guo, "*Ab initio* potential energy surfaces for both the ground (X^1A') and excited (A^1A'') electronic states of HGeBr and the absorption and emission spectra of HGeBr/DGeBr," *Journal of Physical Chemistry A*, vol. 113, no. 26, pp. 7314–7321, 2009.

[20] S. Lin and D. Q. Xie, "New *ab initio* potential energy surfaces for both the ground (X^1A') and excited (A^1A'') electronic states of HSiCl and the absorption and emission spectra of of HSiCl/DSiCl," *Journal of Computational Chemistry*, vol. 32, no. 8, pp. 1694–1702, 2011.

[21] MOLPRO, a package of ab initio programs designed by H.-J. Werner, P. J. Knowles, R. D. Amos et al., version 2006.1.

[22] C. Hampel, K. A. Peterson, and H. J. Werner, "A comparison of the efficiency and accuracy of the quadratic configuration-interaction (QCISD), coupled cluster (CCSD), and Brueckner coupled cluster (BCCD) methods," *Chemical Physics Letters*, vol. 190, no. 1-2, pp. 1–12, 1992.

[23] T. H. Dunning Jr., "Gaussian basis sets for use in correlated molecular calculations. I. The atoms boron through neon and hydrogen," *The Journal of Chemical Physics*, vol. 90, no. 2, pp. 1007–1023, 1989.

[24] S. R. Langhoff and E. R. Davidson, "Configuration interaction calculations on nitrogen molecule," *International Journal of Quantum Chemistry*, vol. 8, no. 1, pp. 61–72, 1974.

[25] P. J. Knowles and H.-J. Werner, "An efficient method for the evaluation of coupling coefficients in configuration interaction calculations," *Chemical Physics Letters*, vol. 145, no. 6, pp. 514–522, 1988.

[26] H.-J. Werner and P. J. Knowles, "An efficient internally contracted multiconfiguration-reference configuration interaction method," *The Journal of Chemical Physics*, vol. 89, no. 9, pp. 5803–5814, 1988.

[27] P. J. Knowles and H.-J. Werner, "An efficient second-order MCSCF method for long configuration expansions," *Chemical Physics Letters*, vol. 115, no. 3, pp. 259–267, 1985.

[28] H.-J. Werner and P. J. Knowles, "A second order multiconfiguration SCF procedure with optimum convergence," *The Journal of Chemical Physics*, vol. 82, no. 11, pp. 5053–5063, 1985.

[29] B. R. Johnson and W. P. Reinhardt, "Adiabatic separations of stretching and bending vibrations: application to H_2O," *The Journal of Chemical Physics*, vol. 85, no. 8, pp. 4538–4556, 1986.

[30] J. C. Light, I. P. Hamilton, and J. V. Lill, "Generalized discrete variable approximation in quantum mechanics," *The Journal of Chemical Physics*, vol. 82, no. 3, pp. 1400–1409, 1985.

[31] C. Lanczos, "An iteration method for the solution of the eigenvalue problem of linear differential and integral operators," *Journal of Research of the National Bureau of Standards*, vol. 45, no. 4, pp. 255–282, 1950.

[32] J. Echave and D. C. Clary, "Potential optimized discrete variable representation," *Chemical Physics Letters*, vol. 190, no. 3-4, pp. 225–230, 1992.

[33] H. Wei and T. Carrington, "The discrete variable representation of a triatomic Hamiltonian in bond length-bond angle coordinates," *The Journal of Chemical Physics*, vol. 97, no. 5, pp. 3029–3037, 1992.

[34] J. V. Lill, G. A. Parker, and J. C. Light, "Discrete variable representations and sudden models in quantum scattering theory," *Chemical Physics Letters*, vol. 89, no. 6, pp. 483–489, 1982.

[35] R. Q. Chen and H. Guo, "A single Lanczos propagation method for calculating transition amplitudes," *The Journal of Chemical Physics*, vol. 111, no. 22, pp. 9944–9951, 1999.

[36] R. Q. Chen and H. Guo, "A single Lanczos propagation method for calculating transition amplitudes. II. Modified QL and symmetry adaptation," *The Journal of Chemical Physics*, vol. 114, no. 4, pp. 1467–1472, 2001.

[37] H. Guo, R. Chen, and D. Xie, "Calculation of transition amplitudes with a single Lanczos propagation," *Journal of Theoretical and Computational Chemistry*, vol. 1, no. 1, pp. 173–185, 2002.